Received: 30 November 2021 | Revised: 29 March 2022 | Accepted: 5 April 2022

DOI: 10.1002/app.52497

RESEARCH ARTICLE

Applied Polymer SCIENCE WILEY

The illumination effects on the current conduction mechanisms of the Au/(Er_2O_3:PVC)/n-Si (MPS) Schottky diodes

Şemsettin Altındal[1] | Yashar Azizian-Kalandaragh[2,3] | Murat Ulusoy[1] | Gholamreza Pirgholi-Givi[4]

[1]Department of Physics, Faculty of Sciences, Gazi University, Ankara, Turkey

[2]Photonics Application and Research Center, Gazi University, Ankara, Turkey

[3]Photonics Department, Applied Science Faculty, Gazi University, Ankara, Turkey

[4]Department of Physics, University of Guilan, Rasht, Iran

Correspondence
Murat Ulusoy, Department of Physics, Faculty of Sciences, Gazi University, Ankara, Turkey.
Email: ulusoymurat@gazi.edu.tr

Funding information
Gazi University Scientific Research Project, Grant/Award Number: GU-BAP.05/2019-26

Abstract

Photoresponse of the Au/(Er_2O_3:PVC)/n-Si diode was executed in a wide range of illumination intensity (P). Its basic electrical parameters such as ideality factor (n), barrier height (Φ_{B0}), series and shunt resistances (R_s, R_{sh}), photocurrent (I_{ph}), energy-dependence of interface states (N_{ss}), and photosensitivity (S) were calculated from the results of the current–voltage (I–V) measurements. At the negative-bias region, an increase in I_{ph} is observed due to the e^--h^+ pairs that occur as a result of increasing P and their drift in opposite directions under the internal electric field. The ln(I_{ph})–ln(P) plot shows a good linear behavior under various applied voltages. Their slopes vary from 1.47 to 1.64, indicating that empty trap levels, that is, levels not occupied by charges, are of low density. The values n, Φ_{B0}, and R_s were obtained using the thermionic emission theory, Cheung, and Norde functions. The value of Φ_{B0} decreases with increasing n and P as linearly with $\Phi_{B0}(n) = (-0.143n + 1.118)$ eV and $\Phi_{B0}(P) = (-2 \times 10^{-4}P + 0.831)$ eV, respectively. This illumination coefficient of Φ_{B0} ($=-2 \times 10^{-4}$ eV/[mW/cm^2]) is close to the temperature coefficient bandgap of Si ($=-4.73 \times 10^{-4}$ eV/K). These results show that the performed Au/(Er_2O_3:PVC)/n-Si diode has excellent photoresponse and can be successfully used in photovoltaic applications instead of conventional metal–semiconductor diodes.

KEYWORDS

Au/n-Si diode with (Er_2O_3:PVC) film, energy-dependent profile of interface states, illumination and voltage dependence of electrical parameters, responsivity/sensitivity

1 | INTRODUCTION

In last years, electrical and optical properties of metal/semiconductor (MS) contacts which are composed of an organic or polymer interlayer, have been investigated as a function of illumination in detail instead of insulator or oxide interlayer because they let modify electrical parameters of them such as ideality factor (n), series/shunt resistances (R_s, R_{sh}), saturation current (I_s or I_0), barrier height (BH), rectification rate (RR), interface/surface states (N_{ss}), photosensitivity (S), open-circuit voltage (V_{oc}).[1–9] All these parameters are usually dependent on the homogeneity of BH, formed interlayer between MS, the density of N_a or N_d, illumination intensity (P), the form of ohmic and rectifier metal contacts, and sample temperature.[10–14] Interface states, located between interlayers and semiconductors, act as recombination centers that can capture and release an electronic charge under

 © 2022 Wiley Periodicals LLC.

illumination and temperature effect. In other words, electronic charges occupy traps in the forbidden bandgap and then migrate from there; hence they act like mobile charges throughout the junction. These states can be originated from the semiconductor-surface imperfection such as dangling bonds, oxygen-vacancies, doping donor/acceptor atoms, periodic disorders in the semiconductor crystal, and some organic contaminations in the laboratory environment during cleaning and preparation processes.[15] Therefore, to reduce the amount of N_{ss}, leakage current, R_s, and increase of BH, RR, and R_{sh}, researchers concentrated on improving the electrical and optical properties by using an organic/polymer interlayer with appropriate metal or metal oxide doped.[16–18] Since polymers were compared with insulators such as SiO_2 and SnO_2, they have conspicuous features such as a good surface area to volume ratio, high charge storage capability, lightweight, strong mechanical and dielectric strength, and simple grown methods. Despite that, unfortunately, polymers have some inabilities, such as dielectric permittivity and poor mobility. However, these disadvantages can be typically overcome by adding some metals (Ni, Co, Zn, Graphene) or metal oxides (MnO, NiO, ZnO) into them.[19–22]

It is seen that the results obtained from the current or capacitance/conductance versus voltage executions generally deviate from their ideal cases owing to the adverse effects of N_{ss}, R_s, and interlayer. For example, in the applications, the C–V plot sometimes shows an apparent peak both in depletion and accumulation regions owing to N_{ss} and R_s, respectively. Similar effects are seen in the ln$I$–V plots. The fact that N_{ss} and the interface deflect these plots away from linearity, especially at higher forward voltage values, is clear proof of their effects and existence.[2,9–13] In semiconductor devices, R_s is usually originated from the bottom ohmic and top Schottky contacts, the use of probe wires from the Schottky contact, the bulk resistance of semiconductor, dislocations and some dirties on semiconductor surface occurred during surface/fabrication preparation, and nonuniform or extremely doped of semiconductor.[10–13] On the other hand, the R_{sh} usually results from physical imperfection such as holes/gaps in the interlayer, high conductivity patches such as grain boundaries/dislocations, leakage current patches along the interlayer between top Schottky and bottom ohmic contacts, and probe wires. Therefore, the voltage applied to the structure contact distributes to the R_s, the interface layer, and the depletion region.

In Schottky diodes (SDs), the bending in the ln$I$–V plots under reverse bias is significantly more apparent than the forward bias values. Because in reverse bias, the internal and external electric fields are in the same orientation depending on the applied voltage. Thus, the total electric field is stronger in this case than in the forward bias. When a diode is exposed to illuminations ($=hc/q\lambda > E_g$), many electron–hole pairs occur at the junction, and electrons may be recombined.[4,23,24] However, the recombination of the electron–hole pairs under the illumination effect decreases, so photocurrent increases in the reverse bias range because of the higher electric field value at the junction.It is well known that the conventional interfacial insulator layer such as SiO_2 formed on a semiconductor surface by the traditional methods (thermal or sputtering) cannot completely passivate the active dangling bonds at the semiconductor surface metal–insulator–semiconductor (MIS) type structures. However, the use of a high dielectric material such as composites of conducting polymer in metal–polymer–semiconductor (MPS) structure can be reduced the active dangling bonds and so leads to a decrease of the leakage current, surface states, series resistance, and increased shunt resistance, BH, and RR.[3,19,22] Therefore, in recent years, conventional MIS structures have been replaced by MPS type structures to improve the quality or performance the MS structures because of some interesting physical properties of polymer or metal-doped polymers are low-cost materials, wide range bandgap and crystallinity, nontoxic, high mechanic-strength, water/alcohol soluble, and can be easy grown methods (sol–gel, electrospinning, spin-coating), when compared insulators. In addition, polymer interlayer can also be easily polarized like insulator material under an external electric field that displaces the charges from their equilibrium position or traps.

Our first aim is to compose MPS type Au/(Er_2O_3:PVC)/n-Si diodes instead of MIS type photodiodes (PDs) due to easily growing the interfacial organic/polymer layer between metal and semiconductor by using a simple spin-coating method when compared insulator layer grown by using traditional methods. The second aim is to investigate basic electrical parameters by utilizing current–voltage (I–V) measurements in the dark and under wide illumination intensities of 50–300 mW/cm^2 by 50 mW/cm^2 steps at room temperature. The voltage-dependent profile of resistance (R_i vs. V) and energy-dependent profile of interface states (N_{ss} vs. E_c-E_{ss}) were also obtained for each illumination intensity. The value of V_{oc}, short circuit current (I_{sc}), filling factor (FF), and efficiency (η) were found as 0.20 V, 0.28 μA, 29.90%, and 0.2% under 100 mW/cm^2 illumination effect, respectively. All obtained parameters of the composed MPS type diode show excellent photo-response and can be successfully used in photovoltaic and solar cell (SC) applications.

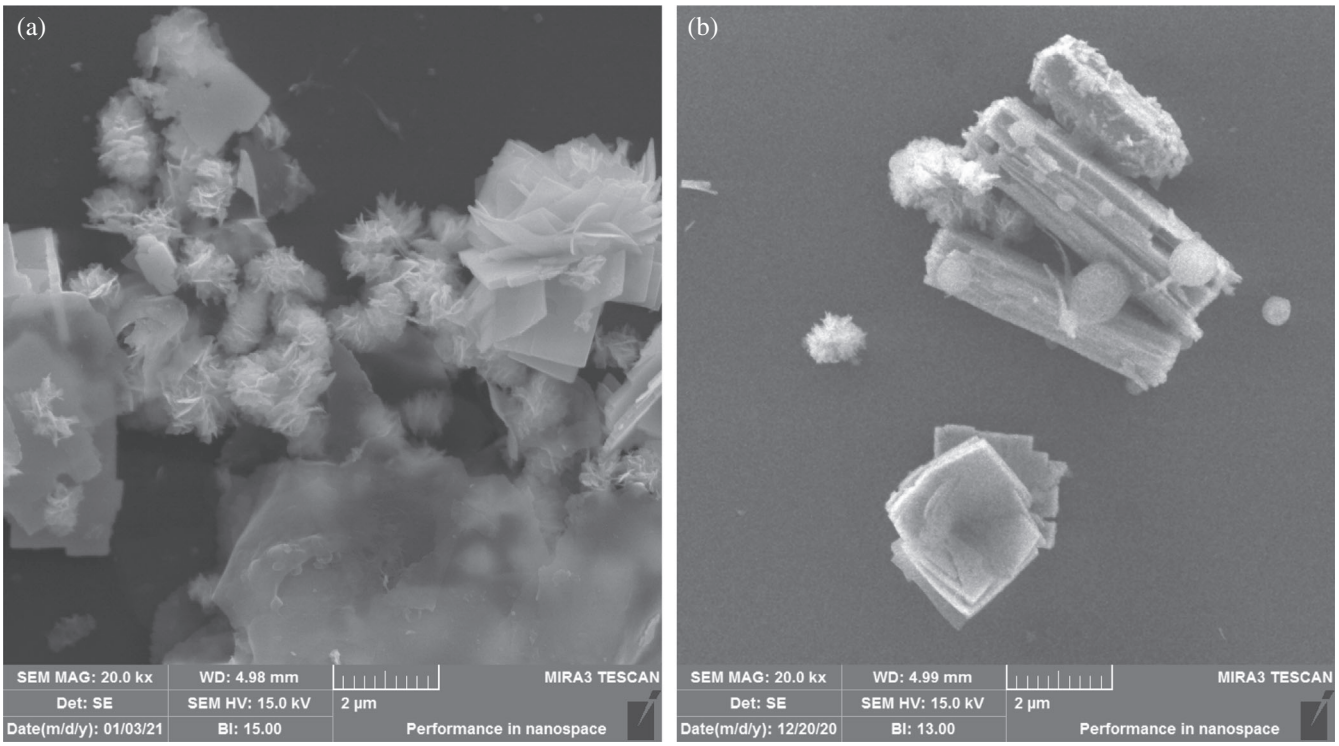


FIGURE 1 (a) The SEM images of the Er_2O_3 and (b) Er_2O_3:PVC nanostructures

2 | EXPERIMENTAL PROCEDURES

Au/(Er_2O_3:PVC)/n-Si diodes have been fabricated onto one-side polished n-Si wafer with 5.08 cm diameter, ~300 μm thickness, <100> float-zone, and 1–10 Ω.cm resistivity. Before the fabrication, the chemical cleaning process was applied to the wafer in the ultrasonic bath by using RCA (Silicon Wafer Cleaning) cleaning procedure. After that, the whole backside of the wafer was thermally coated by high-pure (0.999) Au at 1×10^{-6} Torr. Consequently, the front of the n-Si wafer was rinsed in ($HF + 10H_2O$) chemical solution and then to obstacle perform any native oxide layer at 5 min and dried with pure-N_2 gas. To perform a high-quality ohmic contact backside of the n-Si wafer was treated at 600°C for 4 min in N_2 atmosphere. Then immediately, the prepared (Er_2O_3:PVC) solution was grown on the other side of the wafer via the spin-coating method at 3000 rpm for 1 min. For the preparation of Er_2O_3:PVC film, 0.1 g of Er_2O_3 powder was dissolved in the 10 cc PVC solution. Then Er_2O_3 powders were dispersed in PVC solution under ultrasonic irradiation, and one drop of the mixture onto the other surface of the n-Si wafer. Finally, the high vacuum thermal evaporation system was used to form Au Schottky contacts with a radius of 0.5 mm onto the Er_2O_3:PVC thin polymer layer, obtained 60 nm thickness.

Figure 1(a,b) show the scanning electron microscopy images of the prepared Er_2O_3 and Er_2O_3:PVC samples, respectively. The image shows the formation of flower-like nanostructures and polydispersive structures with thicknesses of each petal are vary from under 200 nm.

Figure 2 shows the EDX analysis of synthesized Er_2O_3 structures. The results show that the ratio of erbium to oxygen is 20:80, which shows a rich amount of oxygen material.

The *I–V* measurements of the SD depending on illumination were executed via Keithley 4200 current/voltage source meter at room temperature. Meantime, Newport–Oriel (Model: 69931) 40–300 W solar simulator was harnessed as the illumination source. The illustration of the Au/(Er_2O_3:PVC)/n-Si diode and its energy band diagram was represented in Figure 3(a,b), respectively.

3 | RESULTS AND DISCUSSION

The semilogarithmic *I–V* curves of the MPS type diode at certain illumination intensities (0–300 mW/cm^2 by 50 mW/cm^2 steps) are shown in Figure 4 in a large voltage range (±5 V). As shown in the figure, all ln*I–V* curves show good rectifying behavior. The curves have good linear behavior at lower positive voltages; however, bendings occur at higher forward bias voltages because of R_s and organic (Er_2O_3:PVC) interfacial layer. Therefore, the current-transport mechanism (CTM) in the moderate forward bias *I–V* range ($V \geq 3kT/q$) has been analyzed through the

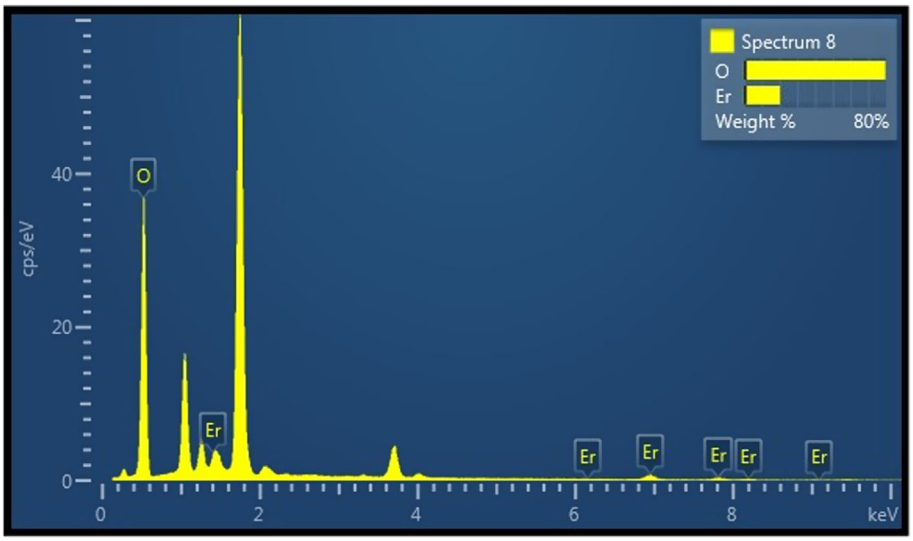


FIGURE 2 The EDX chart of the Er_2O_3 nanostructures [Color figure can be viewed at wileyonlinelibrary.com]

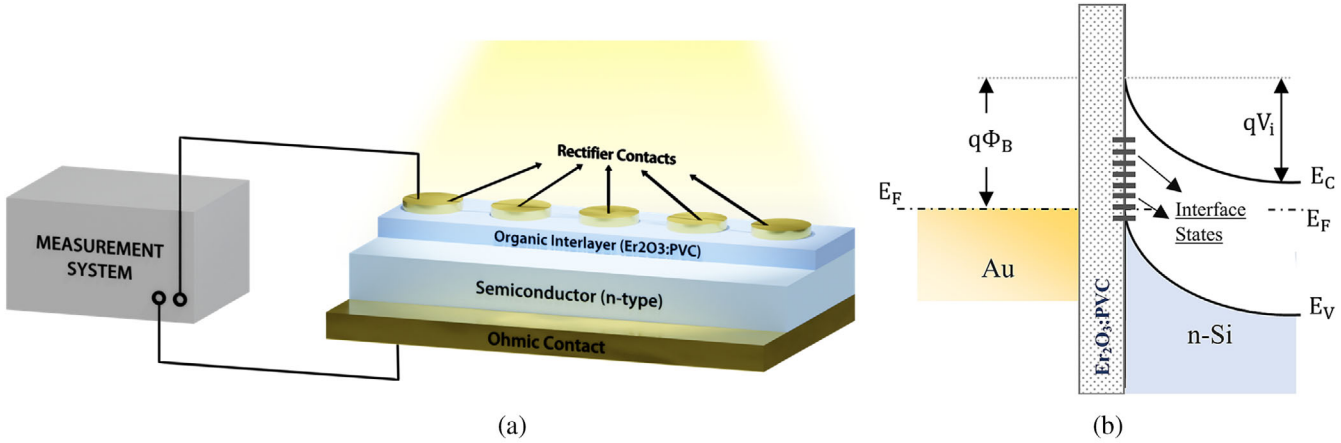


FIGURE 3 (a) The structural schema of the MPS diodes and (b) the schematic energy band diagram of them [Color figure can be viewed at wileyonlinelibrary.com]

standard thermionic emission (TE) theory. Accordingly, when a diode has enough high R_s and $n > 1$, the equation between I and V for the moderate forward bias voltages can be expressed as follows[10,11]:

$$I = \left(AA^*T^2\right)\exp\left(-q\Phi_{B0}/kT\right)\exp\left(\frac{q(V_F - IR_S)}{nkT}\right)\left[1 - \exp\left(\frac{-q(V_F - IR_S)}{kT}\right)\right]. \quad (1)$$

In Equation (1), the IR_s term is the voltage across the R_s of the diode and $AA^*T^2\exp(-q\Phi_{B0}/kT)$ is the reverse saturation-current (I_0), A^* is the effective Richardson constant (=112 A/cm^2.K^2 for n-Si). First, the I_0 values were obtained from the points where the ln$I$–V curves intersect the ln$I$ axis, whose linear regions were determined in the range of approximately 0.24–0.38 V for each illumination intensity and the dark. Then by using the Schottky contact area (=7.85×10^{-3} cm^2) with these values, the zero-bias BH (Φ_{B0}) values were derived from Equation (1), and it is calculated with the equation given below:

$$\Phi_{B0} = \frac{kT}{q}\ln\left(\frac{AA^*T^2}{I_o}\right). \quad (2)$$

The other important electrical parameter n, which is indicative of a deviation from pure TE theory, was also extracted from the slopes of the linear parts of the ln$I$–V curves by using the reverse of thermal energy (kT/q) and slope (=tanθ = $d$ln(I)/dV)) as given below:

$$n = \frac{q}{kT}\left(\frac{dV_F}{d\ln I_F}\right). \quad (3)$$

The values R_s and R_{sh} are also determinants of the forward and reverse bias region I–V characteristics, respectively. Especially the efficiency of PDs and SCs is strongly

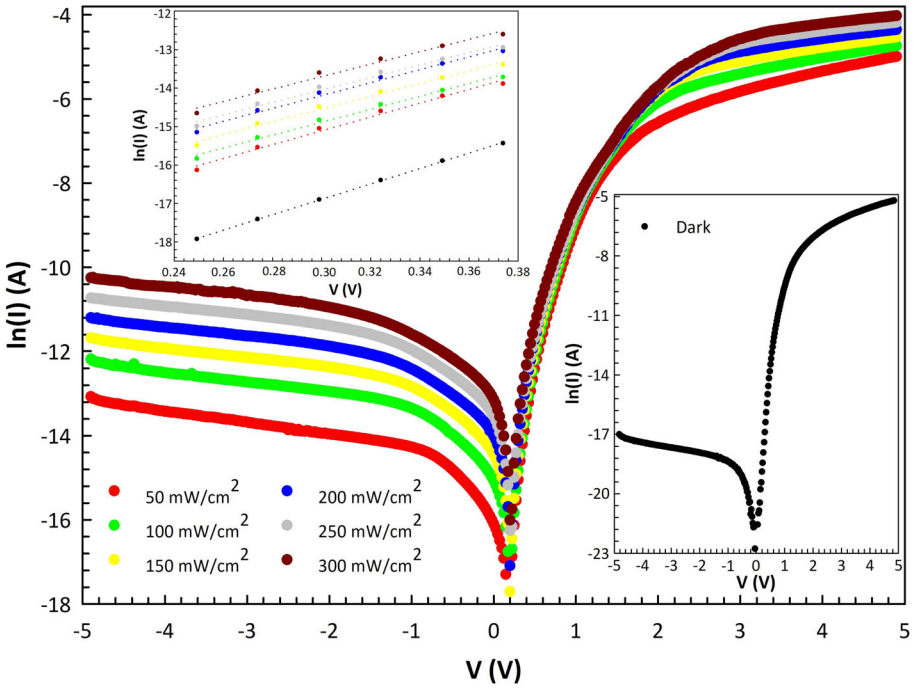


FIGURE 4 The ln*I* versus *V* curves of the MPS diode [Color figure can be viewed at wileyonlinelibrary.com]

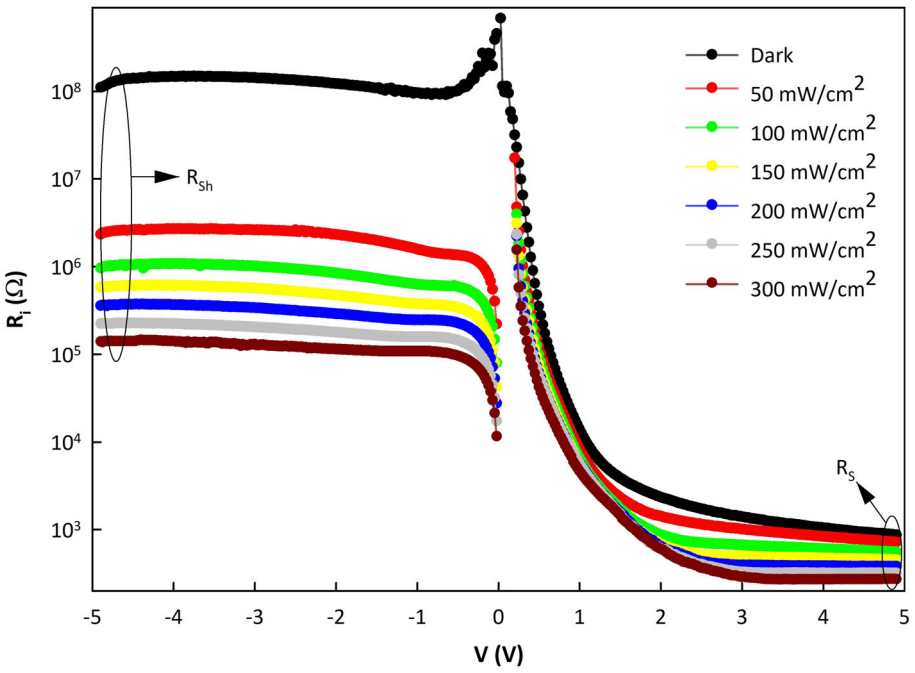


FIGURE 5 The R_i versus *V* curves of the MPS diode [Color figure can be viewed at wileyonlinelibrary.com]

dependent on these two parameters. The resistance changes of the structure (R_i) depending on the voltage can be obtained using Ohm's Law ($R_i = V_i/I_i$); therewithal R_s and R_{sh} values correspond to high forward and reverse bias voltages, respectively. Therefore, the R_i versus *V* curves of the diode were shown in Figure 5. As shown from the figure, the R_s values decreased as a result of the increase in the photocurrent depending on the increasing illumination power. Thus, the determined essential parameters of the diode (I_0, n, Φ_{B0}, R_s, and R_{sh}) from the measurements and the above equations were listed in Table 1.

Table 1 shows that the n and I_0 values increased, and the Φ_{B0}, R_s, and R_{sh} values decreased, depending on the increasing illumination power. Such behavior results from an increase in the photocurrent in both voltage regions. As shown in Figure 6(a), from the plot slope, there is a relation between Φ_{B0} and n given the Φ_{B0} $(n) = (-0.1429n + 1.1183)$ eV equation, and thus the value of Φ_{B0} was calculated as 0.9754 eV for the ideal

TABLE 1 The essential electrical parameters of the MPS diode depends on illumination

P (mW/cm^2)	n	I_0 (A)	Φ_{B0} (eV)	R_s (at +5 V) (Ω)	R_{sh} (at −5 V) (MΩ)
0	1.93	6.93×10^{-10}	0.838	858.39	78.183
50	2.15	1.53×10^{-9}	0.817	709.1	2.089
100	2.21	2.24×10^{-9}	0.807	553.32	0.860
150	2.26	3.35×10^{-9}	0.797	449.96	0.538
200	2.30	4.51×10^{-9}	0.789	381.33	0.350
250	2.35	6.22×10^{-9}	0.781	320.51	0.219
300	2.39	8.85×10^{-9}	0.772	273.89	0.135

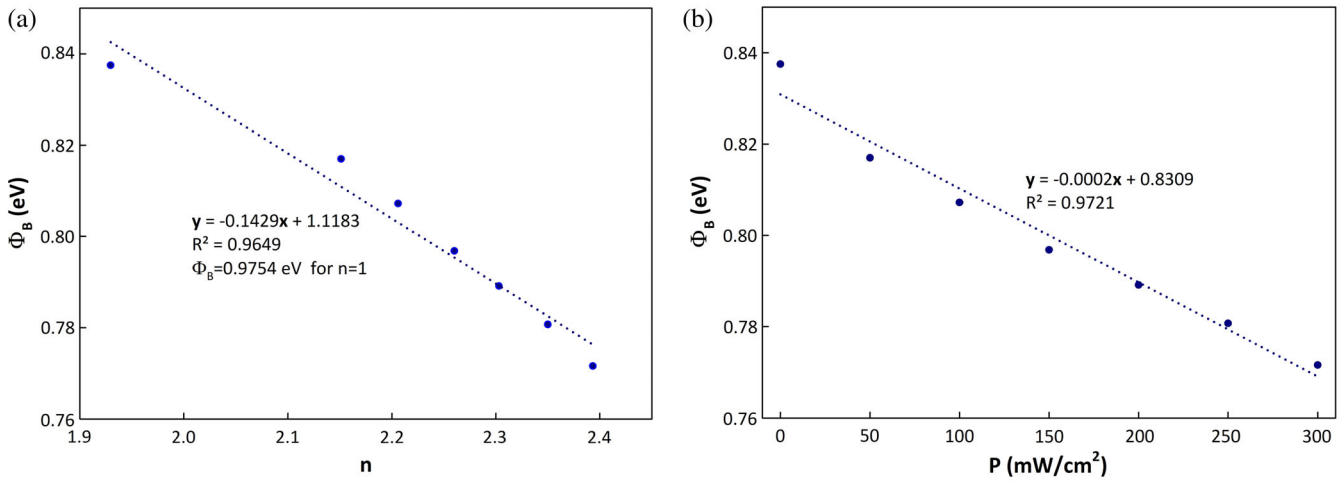


FIGURE 6 (a) The Φ_{B0}-n and (b) Φ_{B0}-P plots of the MPS diode [Color figure can be viewed at wileyonlinelibrary.com]

case ($n = 1$). The fact that the n values calculated for each illumination are higher than the ideal case value is associated with the presence of Er_2O_3:PVC organic interlayer, its thickness, depletion layer width (W_d), the doping concentration of donor atoms (N_d), N_{ss}, and barrier inhomogeneity.[8–12,25,26] There is also a relation between Φ_{B0} and P given the Φ_{B0} $(P) = \Phi_{B0} - \alpha P = (0.831 - 2 \times 10^{-4}P)$ equation from the plot slope of Figure 6(b). This illumination coefficient ($\alpha = d\Phi_{B0}/dP = -2 \times 10^{-4}$) is close to the negative temperature coefficient of the bandgap of Si ($=-4.73 \times 10^{-4}$ eV/K).

When electrons have absorbed enough energy under illumination rather than the E_g, these electrons in the valence-band or interface traps/states can migrate into the conduction-band or trap to the other trap, leading to a photocurrent. The current value for $V = 0$ V and the voltage value for $I = 0$ A are called I_{sc} and V_{oc} under any illumination intensity, respectively. In order to determine the V_{oc}, I_{sc}, FF ($FF = [(V_m I_m)/(V_{oc} I_{sc})]$), and efficiency ($\eta$) of the diode, the efficiency I–V plots were shown in Figure 7 for each illumination. Thus, the efficiency of the SCs or PD can also be calculated by the following relation by using the effective contact area and intensity of illumination (P_{in}) as given follow:

$$\eta = FF \times [(V_{oc} I_{sc})/(P_{in} A)]. \quad (4)$$

Here, I_m and V_m are the current and voltage values corresponding to the maximum power values of the efficiency I–V curves for each illumination intensity. The values of V_{oc}, I_{sc}, FF, and η were found as 0.21 V and 0.28 μA, 29.90%, and 0.22% under 100 mW/cm^2, respectively. This lower value of η results from the presence of R_s and the organic interfacial layer.

The current in the reverse bias voltage is related to the photo conducting behavior. As shown in Figure 8, the photocurrent values (I_{ph}) showed a linear increase at certain negative voltage values depending on the increasing illumination power (P). The following power law gives this linear relation[27–29]:

$$I_{ph} = BP^n, \quad (5)$$

where n is an exponent and B is a constant. The value of n was derived from the slope of $\ln(I_{ph})$–$\ln(P)$ curve for various applied bias voltage (0.0, −0.1, −0.2, −0.3, and −0.4 V), and it changed from 1.473 and 1.644, which indicated a lower density of the unoccupied interface traps.[30–32]

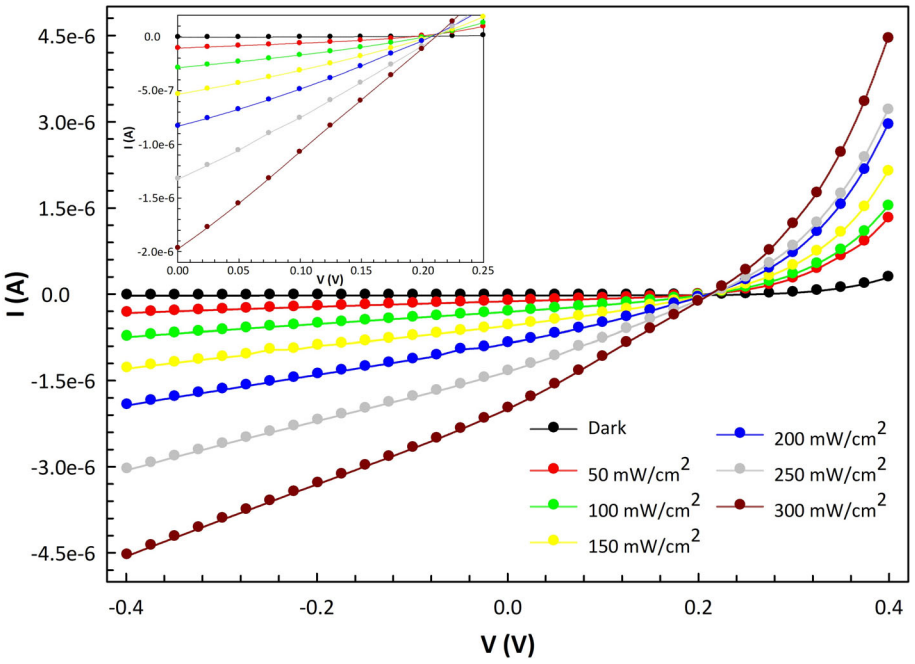


FIGURE 7 The efficiency curves (I vs. V) of the MPS diode [Color figure can be viewed at wileyonlinelibrary.com]

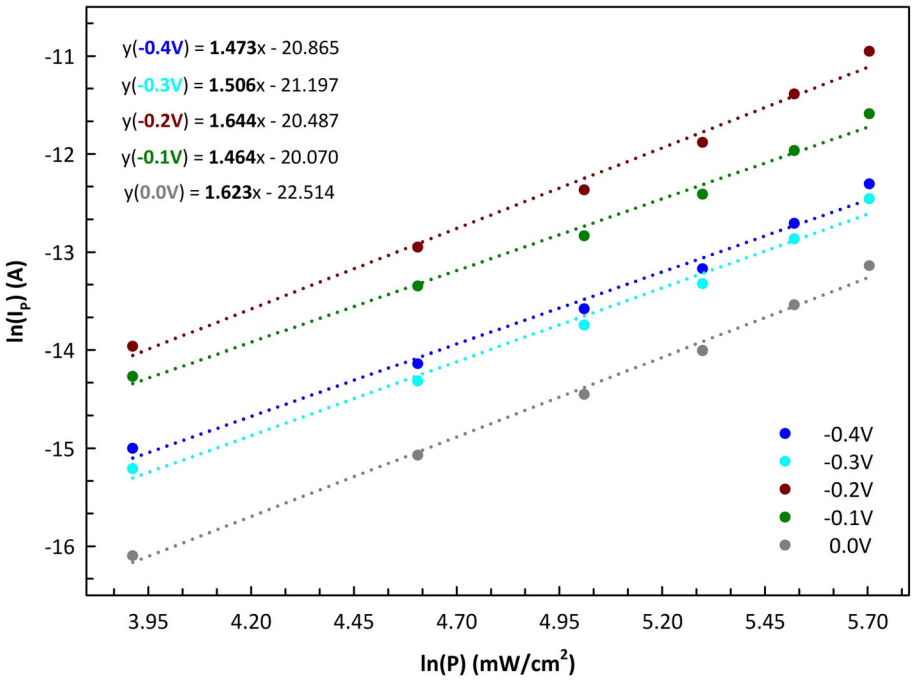


FIGURE 8 The double-logarithmic I_{ph}-P plots of the MPS diode [Color figure can be viewed at wileyonlinelibrary.com]

As shown in Figure 7, the value of photocurrent increase with increasing illumination level. But, the interfacial layer and semiconductor wafer thickness of SCs or PDs is one of the unsolved problems. Therefore, it is necessary to clarify the optimal value of the thickness of the absorbing layer in SCs. When the thickness of the interfacial layer becomes very thin, the absorbing layer leads to a lower photocurrent value. But, the thick interfacial layer leads to large series resistance and leads to a decrease in the photocurrent.

On the other hand, the qualitative characteristics of the SC efficiency for different photoactive layer thicknesses can be obtained by calculating the photocurrent density, taking into account the spectral distribution of solar radiation. As a result, an increase in the interfacial oxide layer thickness leads to an increase in the V_{oc} but a decrease in I_{sc}. Therefore, it is crucial to determine interfacial layer thickness to supply maximum efficiency in SCs or PDs. However, our aim here is to measure the basic battery parameters that affect

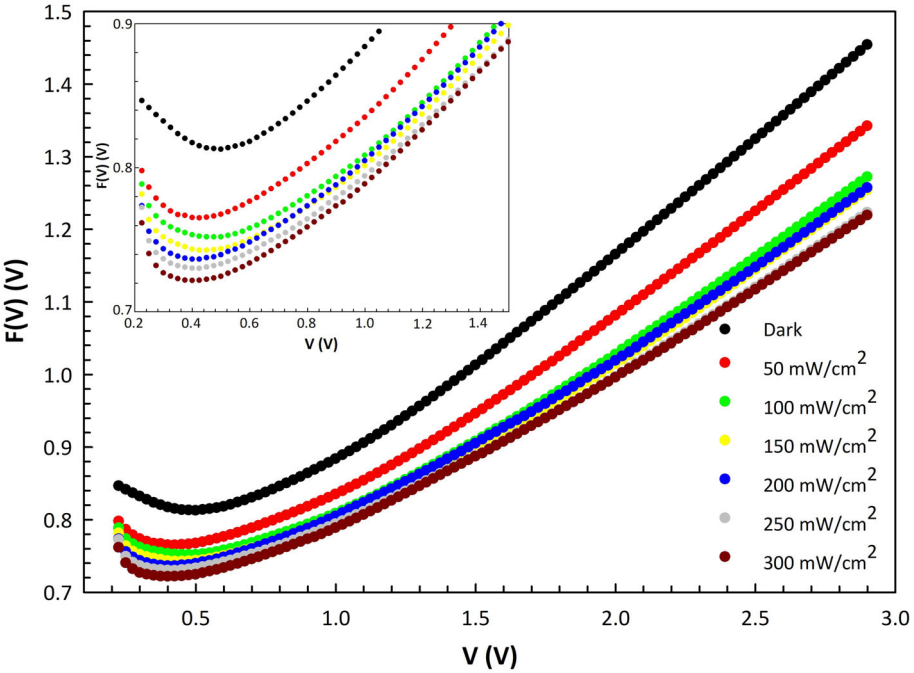


FIGURE 9 The $F(V)$ versus V curves of the MPS diode [Color figure can be viewed at wileyonlinelibrary.com]

TABLE 2 Some essential electrical parameters of the MPS diode using TE, Norde, and Cheung's functions

	I–V			Cheung-I		Cheung-II		Norde	
P (mW/cm^2)	n	Φ_{B0} (eV)	R_s (kΩ)	n	R_s (kΩ)	Φ_{B0} (eV)	R_s (kΩ)	Φ_{B0} (eV)	R_s (kΩ)
0	1.93	0.838	0.86	7.25	0.90	0.664	0.72	0.959	17.73
50	2.15	0.817	0.71	7.27	0.50	0.653	0.40	0.871	15.30
100	2.21	0.807	0.55	8.76	0.23	0.628	0.172	0.856	10.35
150	2.26	0.797	0.45	9.42	0.16	0.617	0.12	0.845	7.81
200	2.30	0.789	0.38	10.10	0.11	0.612	0.09	0.826	10.051
250	2.35	0.780	0.32	10.40	0.08	0.609	0.06	0.823	7.30
300	2.39	0.772	0.27	11.32	0.08	0.596	0.06	0.807	6.94

the efficiency rather than increase the efficiency and investigate the source.

There are some methods in the literature to determine the basic important electrical parameters (n, R_s, and Φ_{B0}), but all of them correspond to different voltage regions. Therefore, these parameters were calculated from the three different methods (TE, Norde, and Cheung's functions), and obtained results were compared. The last two methods are usually used when the forward bias ln$I$ versus V curves do not have enough linear regions. As regards the modified Norde method, the $F(V)$ function is given as follow when $n > 1$[11,33]:

$$F(V) = \frac{V}{\gamma} - \frac{kT}{q} - \left[\ln\left(\frac{I(V)}{AA^*T^2}\right)\right], \tag{6}$$

where γ is an integer and dimensionless, which must be bigger than n. Thus, the values of Φ_{B0} and R_s can be determined through the $F(V)$ versus V curves by use of V_m and I_m values, which correspond to the lowest value of the $F(V)$ versus V curves as given in Figure 9[33]:

$$\Phi_{B0} = F(V_m) + \frac{V_m}{\gamma} - \frac{kT}{q}, \tag{7a}$$

$$R_s = \left(\frac{kT}{q}\right)\left(\frac{\gamma - n}{I_m}\right). \tag{7b}$$

The calculated Φ_{B0} and R_s values from Equations (7a) and (7b) are listed in Table 2. Both the value of Φ_{B0} and R_s increase with decreasing illumination like the TE theory.

The basic values of n, R_s, and Φ_{B0} can also be obtained by following Cheung's functions as another way by using two equations as given follow[34]:

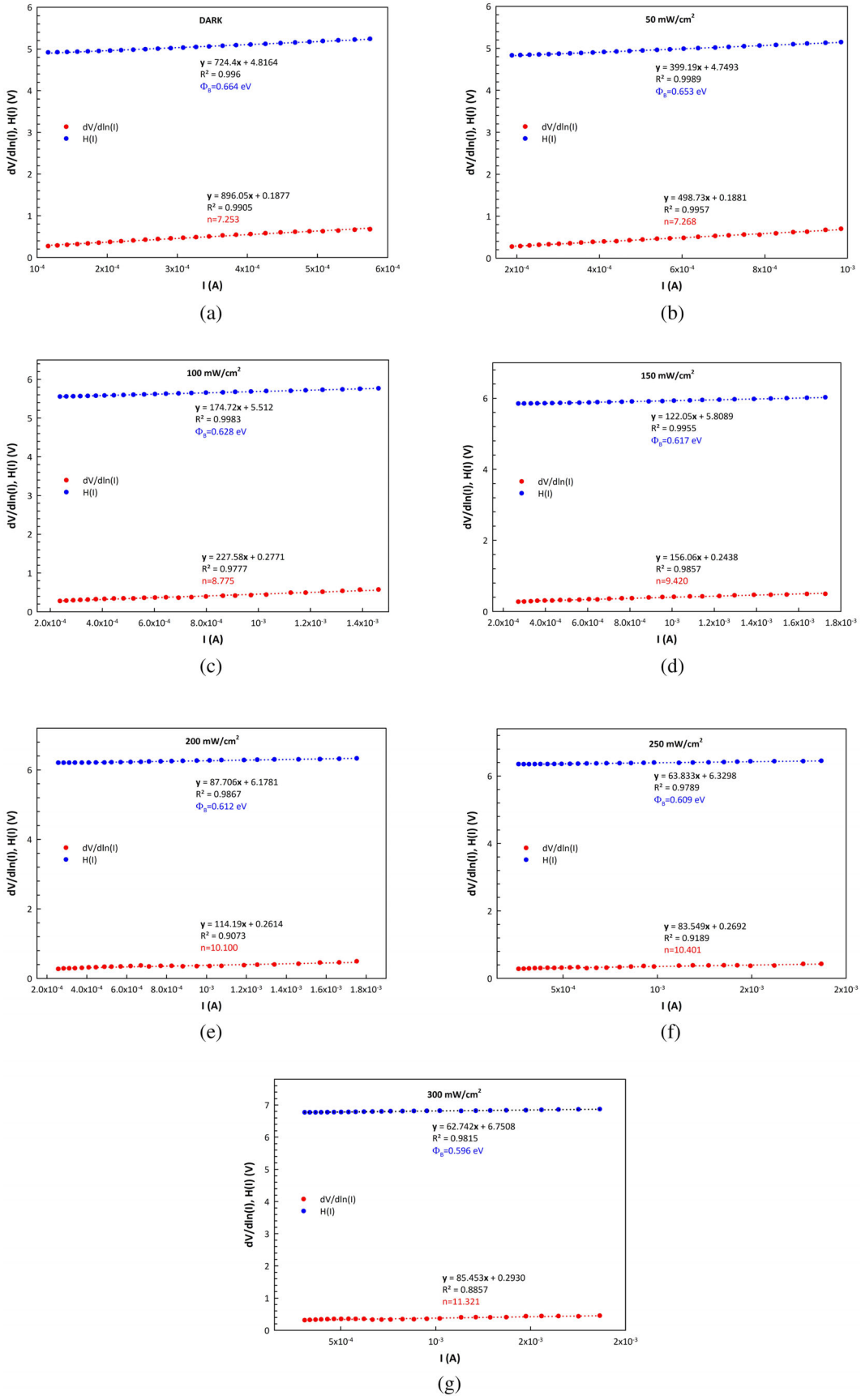


FIGURE 10 (a–g) The dV/dln(I) and $H(I)$ versus I plots of the MPS diode both in the dark and various illumination intensities [Color figure can be viewed at wileyonlinelibrary.com]

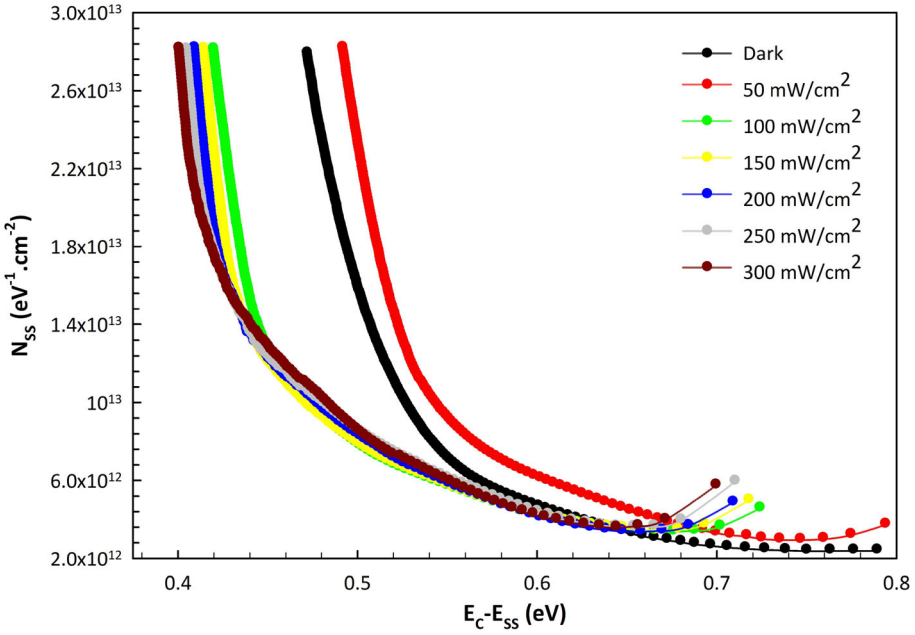


FIGURE 11 The N_{ss} versus (E_c−E_{ss}) curves/profiles of the MPS diode both in the dark and at various illumination intensities [Color figure can be viewed at wileyonlinelibrary.com]

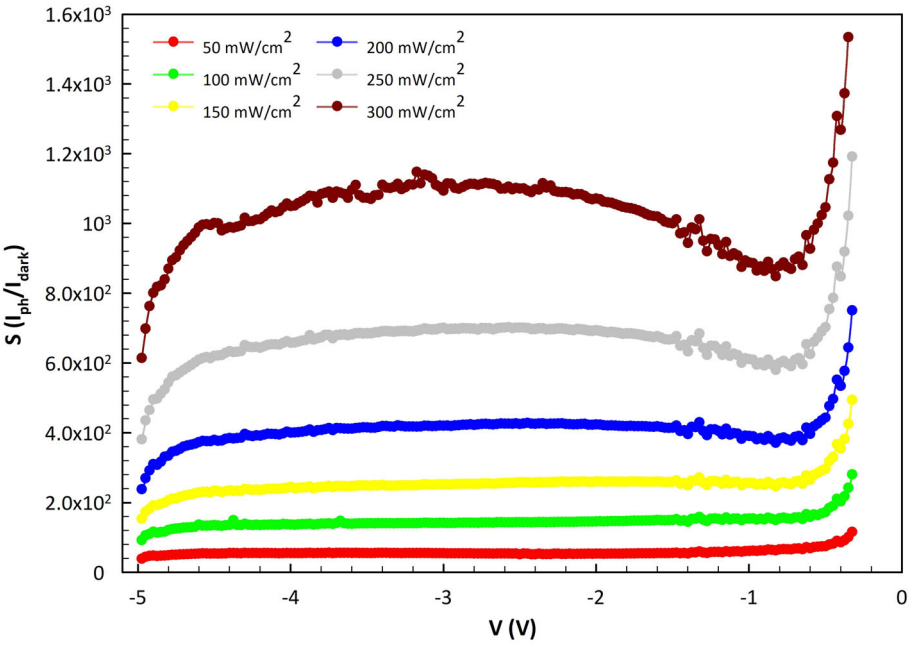


FIGURE 12 The I_{ph}/I_{dark}-V curves of the MPS diode for various illumination [Color figure can be viewed at wileyonlinelibrary.com]

$$dV/d\ln(I) = \frac{nkT}{q} + IR_s, \tag{8a}$$

$$H(I) = V - \frac{kT}{q}\left[\ln\left(\frac{I(V)}{AA^*T^2}\right)\right] = n\Phi_{B0} + IR_s. \tag{8b}$$

The dV/dln(I) and $H(I)$ versus I plots were drawn by use of Equations (8a) and (8b) for the MPS diode in the dark and under six different illumination intensities and then are given in Figure 10(a–g).

Thus, R_s and n values were calculated for the slopes and the intersection point of the dV/dln(I) versus I plots according to Equation (8a). Then using these n values in Equation (8b), $H(I)$ versus I plots were drawn, so R_s and Φ_{B0} values were derived from the slope and intercept point of these plots. In this way, the obtained basic electrical parameters (n, R_s, and Φ_{B0}) of the MPS diode from TE, Norde, and Cheung's methods were listed in Table 2 to see the difference between them. As shown in Table 2, there are differences in the results due to the approaches these methods take into account in obtaining the voltage-dependent parameters.

The existence of N_{ss} between metal and semiconductor is also more effective on the CTM, and it is significantly influential in determining the performance and quality of electronic devices such as MIS, MPS type diodes, and SCs. Therefore, considering the voltage dependence of both

TABLE 3 Some of the identically prepared silicon-based photodiodes with an interfacial polymer layer in the literature and compare some main electrical parameters of them

Photodiodes	V_{oc} (V)	I_{sc} (μA)	*FF* %	*n*	R_s (kΩ)	Φ_{bo} (eV)	Photo-sensitivity
Au/(Er_2O_3:PVC)/n-Si (This study) (Under 100 mW/cm^2)	0.21	0.28	30	2.21	0.23	0.807	1100
Au/($CoFe_2O_4$-PVP)/n-Si[38] (Under 100 mW/cm^2)	—	—	—	4.49	0.43	0.813	400
Au/(rGO-PVP Fs)/p-Si[39] (Under 30 mW/cm^2)	—	—	—	4.43	3.28	0.630	12
Ag/(PVA-MV)/p-Si[40] (Under 80 mW/cm^2)	—	—	—	2.50	—	0.780	322
p-Si/Fe_2-polymeric-complex/Au[41] (Under 100 mW/cm^2)	—	—	—	2.84	7.66	0.687	—
Al/(0.1 coumarin–PVA)/p-Si[20] (Under 100 mW/cm^2)	—	—	—	2.31	0.70	0.770	1686

$\Phi_{B0}(V)$ and $n(V)$, the changes in N_{ss} relative to E_c-E_{ss} were obtained from positive current and voltage values with the equations defined below[35]:

$$n = \frac{q}{kT}\left(\frac{dV}{d(\ln I)}\right) = 1 + \frac{\delta_i}{\varepsilon_i}\left[\frac{\varepsilon_s}{W_D} + qN_{ss}\right], \tag{9a}$$

$$\Phi_e = \Phi_{B0} + \beta(V - IR_s) = \Phi_{B0} + \left(1 - \frac{1}{n(V)}\right)(V - IR_s), \tag{9b}$$

$$E_c - E_{ss} = q\left(\Phi_e - V\right), \tag{9c}$$

$$N_{ss}(V) = \frac{1}{q}\left[\frac{\varepsilon_i}{\delta}(n(V) - 1) - \frac{\varepsilon_s}{W_D}\right]. \tag{9d}$$

In Equations (9a)–(9d), ε_i is the dielectric constant of the interfacial layer, ε_s is the dielectric of the semiconductor, W_D is the thickness of the depletion layer, and δ_i is the thickness of the interfacial layer. As shown in Figure 11, the obtained mean value of N_{ss} at about (E_c−0.55) eV for each illumination intensity is about 10^{13} eV/cm^2.

The observed discrepancies or position in N_{ss} can be explained by the realignments and rearrangements of N_{ss} under illumination and electric field. In other words, as shown in Figure 11, the values of N_{ss} change from $\sim 2.0 \times 10^{12}$ to 2.8×10^{13} (eV/cm^2) almost for each illumination intensity and rise from near the middle bandgap of the semiconductor towards the bottom of the conduction band (E_c). The increase results from reordering and restructuring them under illumination and electric field. The energy states or traps can act as a recombination center that captures and releases an electron depending on illumination intensity and lifetime (τ).

The rates of I_{ph}/I_{dark} which defined photosensitivity (S) in the reverse bias region, were also obtained between −5 and 0 V and shown in Figure 12. As shown in Figure 12, the value of photosensitivity increases with illumination intensity in the measured whole reverse bias region, which is also evidence that the fabricated Au/(Er_2O_3:PVC)/n-Si (MPS) SDs exhibit high photosensitivity in the negative/reverse bias region. Recently, similar results were reported in the literature for MPS type SDs.[22,24,36–38]

Table 3 shows the identically prepared silicon based on some PDs with an interfacial polymer layer in the literature and compares some main electrical parameters under illumination. As can be seen in Table 3, there is a good agreement between the electrical parameters such as n, BH, Rs, and S. The observed difference between them can be attributed to the thickness of the interfacial layer, its permittivity, barrier in-homogeneities between metal and semiconductor, a special density distribution of N_{ss} in the bandgap of semiconductor, voltage dependence of them, and fabrication processes.

4 | CONCLUSION

In this research work, a SD with (Er_2O_3:PVC) organic/polymer interfacial layer grown by the spin-coating method were fabricated instead of (MS) type SDs with an interfacial insulator layer grown by traditional technique. After that, some essential electrical parameters were obtained by utilizing *I–V* measurements first in the dark and then under illuminations up to 300 mW/cm^2 with a regularly increasing value (50 mW/cm^2) starting from 50 mW/cm^2 at room temperature. The double logarithmic I_{ph}–*P* plot shows a good linear behavior under different voltages. Their slopes were changed between 1.47 and 1.64, indicating a lower unoccupied trap/state-level density. The *n*, Φ_{B0}, and R_s were calculated from TE theory, Norde, and Cheung's functions for each illumination intensity to see the voltage-dependent

essential electrical parameters. Experimental results show that the value of Φ_{B0} decreases with increasing n and P as linearly with $\Phi_{B0}(n) = (-0.143n + 1.118)$ eV and $\Phi_{B0}(P) = (-2 \times 10^{-4}P + 0.831)$ eV, respectively. Clearly, this negative illumination coefficient value (-2×10^{-4} eV/[mW/cm^2]) is close to the temperature coefficient bandgap of Si ($=-4.73 \times 10^{-4}$ eV/K). In addition, both the R_i versus V and N_{ss} versus (E_c–E_{ss}) changes were obtained in the dark, and each illumination intensity. For each illumination intensity, the values of V_{oc}, I_{sc}, FF, and η were found as 0.20 V, 0.28 μA, 29.90%, and 0.2% under 100 mW/cm^2, respectively. These results are indicated that the fabricated Au/(Er_2O_3:PVC)/n-Si (MPS) type SDs can be used in photovoltaic and SCs.

AUTHOR CONTRIBUTIONS

Şemsettin Altındal: Supervision (lead); writing – review and editing (lead). **Yashar Azizian-Kalandaragh:** Methodology (lead); resources (lead). **Murat Ulusoy:** Data curation (lead); writing – original draft (equal). **Gholamreza Pirgholi-Givi:** Methodology (equal); resources (equal).

ACKNOWLEDGMENTS

This study was supported by Gazi University Scientific Research Project (Project Number: GU-BAP.05/2019-26).

DATA AVAILABILITY STATEMENT

Research data are not shared.

ORCID

Murat Ulusoy https://orcid.org/0000-0001-9842-0318

REFERENCES

[1] H. Tecimer, T. Tunç, Ş. Altındal, *J. Mater. Sci. Mater. Electron.* **2018**, *29*, 3790.
[2] M. Sharma, S. K. Tripathi, *Appl. Phys. A* **2013**, *113*, 491.
[3] H. G. Çetinkaya, Ö. Sevgili, Ş. Altındal, *Phys. B Condens. Matter* **2019**, *560*, 91.
[4] F. Aslan, H. Esen, F. Yakuphanoglu, *J. Alloys Compd.* **2019**, *789*, 595.
[5] G. Ersöz, İ. Yücedağ, S. Bayrakdar, Ş. Altındal, A. Gümüş, *J. Mater. Sci. Mater. Electron.* **2017**, *28*, 6413.
[6] P. Kumar, S. C. Jain, V. Kumar, S. Chand, R. P. Tandon, *Appl. Phys. A* **2009**, *94*, 281.
[7] S. O. Tan, H. Uslu Tecimer, O. Çiçek, H. Tecimer, İ. Orak, Ş. Altındal, *J. Mater. Sci. Mater. Electron.* **2016**, *27*, 8340.
[8] S. Demirezen, *J. Mater. Sci. Mater. Electron.* **2019**, *30*, 854.
[9] S. Demirezen, İ. Orak, Y. Azizian-Kalandaragh, Ş. Altındal, *J. Mater. Sci. Mater. Electron.* **2017**, *28*, 967.
[10] S. M. Sze, K. K. Ng, *Physics of Semiconductor Devices*, 3rd ed., John Wiley & Sons, Inc., Hoboken, NJ **2006**.
[11] B. L. Sharma, in *Metal–Semiconductor Schottky Barrier Junctions and Their Applications* (Ed: B. L. Sharma), Springer US, Boston, MA **1984**.
[12] J. H. Werner, H. H. Güttler, *J. Appl. Phys.* **1991**, *69*, 1522.
[13] Nicollian, E. H.; Brews, J. R. *MOS (Metal Oxide Semiconductor) Physics and Technology*. John Wiley & Sons, New Jersey **2002**.
[14] S. Demirezen, Ş. Altındal, İ. Uslu, *Curr. Appl. Phys.* **2013**, *13*, 53.
[15] M. S. P. Reddy, P. T. Puneetha, Y.-W. Lee, S.-H. Jeong, C. Park, *Polym. Test.* **2017**, *59*, 107.
[16] İ. Orak, K. Ejderha, A. Turut, *Curr. Appl. Phys.* **2015**, *15*, 1054.
[17] O. Çiçek, S. O. Tan, H. Tecimer, Ş. Altındal, *J. Electron. Mater.* **2018**, *47*, 7134.
[18] O. Çiçek, H. Uslu Tecimer, S. O. Tan, H. Tecimer, İ. Orak, Ş. Altındal, *Compos. Part B* **2017**, *113*, 14.
[19] H. G. Çetinkaya, Ş. Altındal, I. Orak, I. Uslu, *J. Mater. Sci. Mater. Electron.* **2017**, *28*, 7905.
[20] S. Demirezen, S. Altındal Yerişkin, *Polym. Bull.* **2020**, *77*, 49.
[21] M. Siva Pratap Reddy, K. Sreenu, V. Rajagopal Reddy, C. Park, *J. Mater. Sci. Mater. Electron.* **2017**, *28*, 4847.
[22] V. R. Reddy, *Thin Solid Films* **2014**, *556*, 300.
[23] A. Tataroğlu, O. Dayan, N. Özdemir, Z. Serbetci, A. A. Al-Ghamdi, A. Dere, F. El-Tantawy, F. Yakuphanoglu, *Dyes Pigments* **2016**, *132*, 64.
[24] A. Tataroğlu, Ş. Altındal, Y. Azizian-Kalandaragh, *J. Mater. Sci. Mater. Electron.* **2020**, *31*, 665.
[25] R. K. Gupta, K. Ghosh, P. K. Kahol, *Physica E* **2009**, *41*, 617.
[26] İ. Dökme, Ş Altindal, İ. Uslu, *J. Appl. Polym. Sci.* **2012**, *125*, 1185.
[27] A. Dere, B. Coskun, A. Tataroğlu, A. G. Al-Sehemi, A. A. Al-Ghamdi, H. M. A. Alateeq, R. Qindeel, W. A. Farooq, F. Yakuphanoglu, *Phys. B Condens. Matter* **2018**, *545*, 86.
[28] S. Demirezen, H. G. Çetinkaya, M. Kara, F. Yakuphanoğlu, Ş Altındal, *Sensors Actuators A Phys.* **2021**, *317*, 449.
[29] B. P. Rand, J. Genoe, P. Heremans, J. Poortmans, *Prog. Photovolt. Res. Appl.* **2007**, *15*, 659.
[30] R. AL-Wafi, *Silicon* **2018**, *10*, 1639.
[31] O. Sevgili, *Solid State Sci.* **2021**, *117*, 635.
[32] D. E. Yıldız, S. Karadeniz, H. H. Gullu, *J. Mater. Sci. Mater. Electron.* **2021**, *32*, 130.
[33] H. Norde, *J. Appl. Phys.* **1979**, *50*, 5052.
[34] S. K. Cheung, N. W. Cheung, *Appl. Phys. Lett.* **1986**, *49*, 85.
[35] H. C. Card, E. H. Rhoderick, *J. Phys. D. Appl. Phys.* **1971**, *4*, 4.
[36] F. Ş Kaya, S. Duman, İ. Orak, Ö. Baris, *Mater. Sci. Eng. B* **2021**, *265*, 980.
[37] A. Yeşildağ, M. Erdoğan, Ö. Sevgili, Z. Çaldıran, İ. Orak, *J. Electron. Mater.* **2021**, *50*, 6448.
[38] A. B. Ulusan, A. Tataroglu, Ş Altındal, Y. Azizian-Kalandaragh, *J. Mater. Sci. Mater. Electron.* **2021**, *32*, 732.
[39] S. Khalili, H. M. Chenari, F. Yıldırım, Z. Orhan, S. Aydogan, *J. Alloys Compd.* **2021**, *889*, 647.
[40] A. M. El-Mahalawy, M. A.-E. Salam, *Appl. Phys. A* **2020**, *126*, 393.
[41] B. Gündüz, N. Turan, E. Kaya, N. Çolak, *Synth. Met.* **2013**, *184*, 73.

How to cite this article: Ş Altındal, Y. Azizian-Kalandaragh, M. Ulusoy, G. Pirgholi-Givi, *J. Appl. Polym. Sci.* **2022**, e52497. https://doi.org/10.1002/app.52497